Analytic calculation of polarized neutron reflectivity from superconductors

Huai Zhang and J. W. Lynn
Center for Superconductivity Research, Department of Physics, University of Maryland, College Park, Maryland 20742 and Reactor Radiation Division, National Institute of Standards and Technology, Gaithersburg, Maryland 20899
(Received 30 April 1993)

We have obtained an analytic expression for the reflectivity $R^{\pm}(\theta,\lambda)$ of polarized neutrons from a superconductor in the Meissner state, where λ is the magnetic-field penetration depth and θ is the incident angle of the neutron beam. The result is derived as an exact solution of the 1D Schrödinger equation in the continuum limit, with an interaction potential $V^{\pm}(x)=V_N\pm\mu H[\exp(-x/\lambda)-1]$, where V_N is a constant representing the nuclear interaction, μ is the neutron magnetic moment, and H is the applied magnetic field. The solution for $R^{\pm}(\theta,\lambda)$ reveals surprising features in its λ dependence that have not been discovered in previous numerical studies. In particular, $R^{-}(\theta,\lambda)$ displays an oscillatory dependence on λ within a narrow angular range immediately above the total reflection angle ($\theta\gtrsim\theta_c^-$), instead of a monotonic dependence as inferred from earlier numerical calculations. The solution also reveals that complete transmission for the down-spin state [$R^{-}(\theta,\lambda)=0$] may occur when λ and H satisfy certain conditions. In addition to the analytic expression of the reflectivity for a semi-infinite sample, we have also obtained the reflectivity $\tilde{R}^{\pm}(\theta,\lambda)$ from a thick superconducting film where the magnetic field can penetrate from both sides. In the case of a free-standing film of which the two surfaces are identical, we have simply $\tilde{R}^{\pm}=2R^{\pm}/(1+R^{\pm})$, and therefore all the interesting features of the exact solution $R^{\pm}$ persist in $\tilde{R}^{\pm}$. Finally, the exact solution can also be applied to other systems where the scattering potential has an exponential dependence with distance, such as for the magnetization at the surface of a ferromagnet.

I. INTRODUCTION

In the last decade polarized neutron reflectometry has been developed into a new technique to measure the magnetic-field penetration depth λ in superconductors.[1-8] The merit of the method lies in the fact that it provides an *absolute* measurement of λ rather than providing a relative measure as a function of temperature, and therefore neutron reflectometry has the potential to make a model-independent determination of $\lambda(T)$. In 1984, Felcher *et al.*[1] demonstrated in an experiment on superconducting niobium that polarized neutron reflectivity $R^{\pm}$ could be used to measure the magnetic penetration depth. Subsequent experiments were carried out on pure lead and lead-bismuth films.[2,5] Following the advent of high-T_c superconductors, measurements on $YBa_2Cu_3O_{7-x}$ samples were also reported.[3,4] Recently, more investigations in the Nb system were published.[6,7] All these experiments demonstrated that spin-polarized neutron reflectivity is sensitive to the screening of the magnetic field inside a superconductor.

To calculate the expected neutron reflectivity the scattering theory is often cast in the form of a neutron "optical potential," where the three-dimensional (3D) periodic nuclear scattering potential is approximated by the average nuclear potential of a continuum. This procedure is identical to the description of an electromagnetic wave in a material, where the 3D distribution of electrons is replaced by an optical index of refraction. Generally it is an excellent approximation when the wavelength is large compared to the interatomic spacings. Then for the case of neutrons impinging on a flat surface (usually at glancing angles) the scattering can be described by a one-dimensional (1D) Schrödinger equation. In optical terms, the index of refraction for the magnetic and nuclear scattering is given by[9]

$$n=\left[1-\frac{N\lambda_n^2}{\pi}(b\pm p)\right]^{1/2}, \tag{1}$$

where b is the average coherent nuclear scattering amplitude, N is the number density, p is the magnetic scattering amplitude, λ_n is the neutron wavelength, and the $\pm$ refers to incident neutrons with spin up or spin down. Equation (1) is an excellent approximation for describing neutron scattering from a surface in the vicinity of the critical angle θ_c, given by

$$\theta_c=\sin^{-1}\left[\frac{N\lambda_n^2}{\pi}(b\pm p)\right]^{1/2}\approx\left[\frac{N\lambda_n^2}{\pi}(b\pm p)\right]^{1/2}. \tag{2}$$

Below θ_c we have total external reflection of the neutrons, and the reflectivity is unity. For thermal and cold neutrons these angles are quite small; for example, for the nuclear scattering at a neutron wavelength of $\lambda_n=2.35$ Å, $\theta_c=0.151°$ for niobium and 0.167° for $YBa_2Cu_3O_7$, and hence we may make the approximation as in the right-hand side of Eq. (2). For very cold and ultracold neutrons, on the other hand, the angle is not small and the full expression must be used.

For the magnetic interaction the field inside the superconductor is assumed to have the familiar (London) exponential decrease with distance below the first critical field H_{c1};[10]

 ©1993 The American Physical Society

$$\mathbf{B}(x)=\mathbf{H}\exp(-x/\lambda)\ . \tag{3}$$

This local-interaction form for the screening is characteristic of type-II superconductors in their Meissner state, where λ is related to the London penetration depth λ_L in various ways depending on its size relative to the superconducting coherent length ξ_0 and the electron's normal-state mean free path l due to impurities and defects.[11] Since the values for H_{c1} are typically quite small, the magnetic interaction $-\boldsymbol{\mu}\cdot\mathbf{B}$ that arises from Eq. (3) is small compared to the nuclear interaction, and hence below T_c the ratio of the spin-dependent reflectivities R^+/R^- deviates significantly from unity only in the regime just above the critical angle. This is just the regime where the continuum approximation works very well. Typically the deviation was then calculated by numerically solving the optical equation with a refractive index[1,2]

$$n^{\pm}(x)=1-\left[\frac{\lambda_n^2}{2\pi}\right]\left\{Nb\mp cH\left[1-\exp\left[-\frac{x}{\lambda}\right]\right]\right\}, \tag{4}$$

where $c=2\pi\mu m/h^2=2.31\times10^{-10}$ Å^{-2}Oe^{-1}, and the value of λ was obtained by fitting the model calculation for the reflectivity to the experimental data.

Due to the numerical nature of the calculations, details of the λ dependence of the reflectivity $R^{\pm}$ were not analyzed explicitly. The only analytical expression has been obtained in the regime far away from total reflection, using the Born approximation.[1,2] This expression was then extrapolated to the region of the critical angle as an attempt to theoretically analyze the λ dependence of $R^{\pm}$. From such analysis it was believed that $\Delta R=R^+-R^-$ at the critical angle was the same irrespective of the shape of $B(x)$, and only for larger angles of incidence did the shape of the magnetic profile become important. It was also believed that the effect of a smoother variation of $B(x)$ was to decrease ΔR. However, in spite of the paucity of analytical results, the often successful quantitative fits of the numerical calculations to the experimental data provided a competitive technique to measure the magnetic-field penetration depth λ in superconductors.

In this paper we use the same basic approach of calculating the neutron reflectivity in terms of an optical potential. We have solved the 1D Schrödinger equation, and found an analytical solution for $R^{\pm}(\theta,\lambda)$ which is valid throughout the entire angular range of interest. We study some of the features of this solution. In addition, we have obtained an analytic expression for the reflectivity from a thick film, $\tilde{R}^{\pm}(\theta,\lambda)$, which relates to that from a semi-infinite sample, $R^{\pm}(\theta,\lambda)$, in a simple and elegant way. This makes the theoretical predictions easier to compare with experiment. We note that preliminary results of this work have been reported earlier.[8]

II. CALCULATION OF $R^{\pm}(\theta,\lambda)$

We start with the Schrödinger equation describing a neutron incident on a plane-surfaced and semi-infinite superconducting sample placed in an applied magnetic field $\mathbf{H}$;

$$-(\hbar^2/2m)\nabla^2\Psi(\mathbf{x})+V(\mathbf{x})\psi(\mathbf{x})=E\Psi(\mathbf{x})\ . \tag{5}$$

If we approximate the periodic arrangement of nuclei in the sample by a homogeneous continuum, then we have translational symmetry in the yz plane and only the x component of $\mathbf{k}$, $k_x=k\sin\theta$, can change. Hence we have a classic quantum-textbook 1D problem; to the incoming neutron the sample is represented as a simple potential barrier which consists of the neutron's nuclear interaction with the average nuclear scattering potential and its magnetic interaction with the magnetic inductance in the sample. Thus we have

$$V(x)=V_N(x)+V_M(x) \tag{6}$$

with the nuclear and magnetic potentials given by

$$\left.\begin{aligned}V_N(x)&=\left[\frac{2\pi\hbar^2}{m}\right]Nb\equiv V_N\\ V_M(x)&=-\boldsymbol{\mu}\cdot\mathbf{H}\exp\left[-\frac{x}{\lambda}\right]\end{aligned}\right\},\quad x>0 \tag{7}$$

and

$$\left.\begin{aligned}V_N(x)&=0\\ V_M(x)&=-\boldsymbol{\mu}\cdot\mathbf{H}\end{aligned}\right\},\quad x<0\ . \tag{8}$$

This is of course an idealized potential, where we neglect such processes as nuclear absorption, incoherent and phonon scatterings, surface roughness, etc. Since the potential for $x<0$ is a constant, one can make it zero and take the change of the potential at the surface as an effective potential for $x>0$:

$$V^{\pm}(x)=V_N\pm\mu\cdot H[\exp(-x/\lambda)-1]\ , \tag{9}$$

where the $\pm$ refers to incident neutrons with spin up or spin down. $V^{\pm}(x)$ is primarily a potential step, since the magnetic interaction for fields below H_{c1} is typically two orders of magnitude smaller. When θ is small enough such that $\hbar^2k_x^2/2m$ is below this potential step the neutron is unable to overcome the barrier and therefore is totally reflected. When θ exceeds the critical angle then the neutron has a probability for both reflection and transmission. The reflectivity $R^{\pm}(\theta)$ depends of course on the details of the magnetic term in $V^{\pm}(x)$, particularly when θ is near the critical angle, and hence a measurement of $R^{\pm}(\theta)$ can serve to determine the magnetic-field penetration depth λ. We note that for thermal and cold neutrons θ_c is typically below 1°, and this is the conventional regime for neutron reflectometers,[2,3,12] while for very cold neutrons θ_c can be much larger than 1°, and for ultracold neutrons $\theta_c\rightarrow\pi/2$.[13] The calculation we present below applies to all these cases.

We define

$$u_N=4\pi Nb \tag{10}$$

and

$$u_M=\begin{cases}+2\mu Hm/\hbar^2=+4\pi cH\geq0 & \text{for spin up}\\ -2\mu Hm/\hbar^2=-4\pi cH\leq0 & \text{for spin down}\ ,\end{cases} \tag{11}$$

where $c\equiv2\pi\mu m/h^2$. Then the Schrödinger equation becomes

$$\nabla^2\Psi(\mathbf{x})+\{k'^2-u_N+u_M[1-\exp(-x/\lambda)]\}\Psi(\mathbf{x})=0 , \tag{12}$$

where

$$k'=(k^2-u_M)^{1/2} . \tag{13}$$

We have defined k' to emphasize the point that the kinetic energy of the incoming neutrons might be spin dependent depending on the way the polarized neutrons are prepared. If the external magnetic field changes gradually from (essentially) zero to H over a macroscopic distance, the neutrons are not scattered at all but only adiabatically tuned into a different energy. For thermal or cold neutrons $k'=k$ to a very good approximation; for example, with $\lambda_n=2.35$ Å and $H=500$ Oe we have $k^2=7.15$ Å^{-2} and $|u_M|=1.45\times10^{-6}$ Å^{-2}. Therefore we may neglect the difference between k and k'. In the case of ultracold neutrons, on the other hand, the kinetic and potential energies are comparable, and in this case one can simply replace k by k' if necessary for each spin state as given in Eq. (11). Hence, we will drop the distinction between k and k' from further discussion.

Due to the translational symmetry of the scattering potential in both y and z directions near the sample surface, Eq. (12) can be reduced to a 1D equation by the standard procedure of separating variables. We have

$$\frac{d^2\Psi(x)}{dx^2}+[k_x^2-u(x)]\Psi(x)=0 \tag{14}$$

with

$$u(x)=\begin{cases}0 , & x<0\\ u_N-u_M[1-\exp(-x/\lambda)] , & x\geq 0 .\end{cases} \tag{15}$$

Figure 1 shows sketches of $u(x)$ for spin-up and spin-down neutrons.

In the region $x\geq 0$ we define

$$\kappa\equiv+(k_x^2-u_N+u_M)^{1/2} . \tag{16}$$

Then Eq. (14) becomes

$$\frac{d^2\Psi(x)}{dx^2}+[\kappa^2-u_M\exp(-x/\lambda)]\Psi(x)=0 . \tag{17}$$

Letting

$$\Psi(x)\equiv\Phi(x)\exp(i\kappa x) , \tag{18}$$

we obtain an equation for $\Phi(x)$:

$$\frac{d^2\Phi(x)}{dx^2}+2i\kappa\frac{d\Phi(x)}{dx}-u_M\exp(-x/\lambda)\Phi(x)=0 . \tag{19}$$

The expected asymptotic behavior that $\Psi(x)\rightarrow t\exp(i\kappa x)$ as $x\rightarrow+\infty$ imposes the boundary condition on $\Phi(x)$ that $\Phi(x)\rightarrow t$ as $x\rightarrow+\infty$, where t is a constant, which turns out to be the transmission amplitude. Changing variables to

$$\xi\equiv\lambda^2u_M\exp(-x/\lambda) , \tag{20}$$

where λ is positive definite, we have

$$\xi\frac{d^2\Phi}{d\xi^2}+(1-2i\kappa\lambda)\frac{d\Phi}{d\xi}-\Phi=0 . \tag{21}$$

Now we can make a series expansion of Φ in ξ; we find that the solution to Eq. (21) is

$$\Phi=t\,{}_0F_1(1-2i\kappa\lambda;\xi) , \tag{22}$$

where t is an undetermined coefficient and ${}_0F_1$ is a generalized hypergeometric function defined as[14]

$${}_0F_1(\alpha;z)\equiv\sum_{n=0}^{+\infty}\frac{\Gamma(\alpha)z^n}{\Gamma(\alpha+n)n!} \tag{23}$$

for all z. The solution of $\Psi(x)$ in the $x\geq 0$ region is then

$$\Psi(x)=t\,{}_0F_1[1-2i\kappa\lambda;\lambda^2u_M\exp(-x/\lambda)]\exp(i\kappa x) . \tag{24}$$

We need a minimum set of relations pertaining to the generalized hypergeometric function ${}_0F_1$ for our discussion. Several relations for special values of ${}_0F_1$ can be easily derived from Eq. (23):

$${}_0F_1(\alpha;0)=1 , \tag{25a}$$

$${}_0F_1(1;z)=J_0(2|z|^{1/2}) \quad \text{if } z\leq 0 , \tag{25b}$$

$${}_0F_1(1;z)=I_0(2z^{1/2}) \quad \text{if } z\geq 0 , \tag{25c}$$

$${}_0F_1(2;z)=\frac{J_0(2|z|^{1/2})}{|z|^{1/2}} \quad \text{if } z\leq 0 , \tag{25d}$$

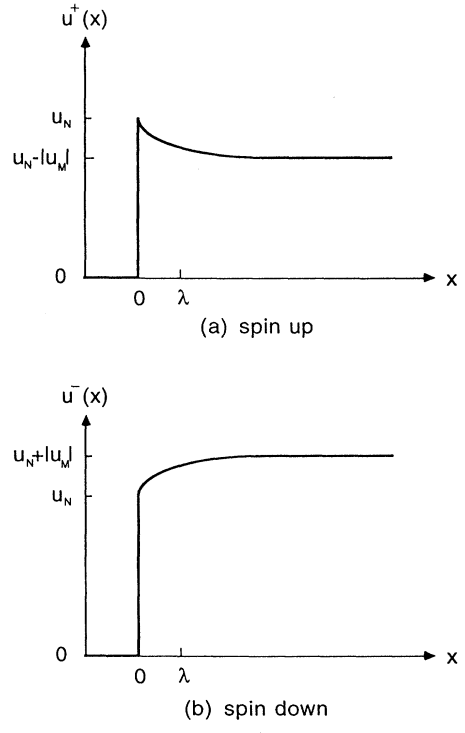

FIG. 1. Sketch of the interaction potential $u(x)$ for spin-up neutrons (a) and spin-down neutrons (b), defined by Eq. (15). The subscripts N and M indicate nuclear and magnetic interactions, respectively. Note that u_N and $|u_M|$ have not been drawn to scale here, as $|u_M|$ is typically two orders of magnitude smaller than u_N.

$$ {}_0F_1(2;z)=\frac{I_0(2z^{1/2})}{z^{1/2}} , \quad \text{if } z\geq 0 , \tag{25e} $$

where J_n is the nth-order Bessel function and I_n the nth-order modified Bessel function. The first-order partial derivatives of ${}_0F_1(\alpha;z)$ with respect to α and z are

$$ {}_0F'_{1,1}(\alpha;z)\equiv\frac{\partial}{\partial\alpha}{}_0F_1(\alpha;z) $$

$$ =-\sum_{n=1}^{+\infty}\frac{\Gamma(\alpha)z^n}{\Gamma(\alpha+n)n!}\sum_{m=0}^{n-1}\frac{1}{\alpha+m} ; \tag{26a} $$

$$ {}_0F'_{1,2}(\alpha;z)\equiv\frac{\partial}{\partial z}{}_0F_1(\alpha;z)=\frac{1}{\alpha}{}_0F_1(\alpha+1;z) . \tag{26b} $$

Now let us consider the boundary conditions. As $x\rightarrow+\infty$, $\xi\rightarrow 0$, and we have ${}_0F_1(1-2i\kappa\lambda;\xi)\rightarrow 1$ and hence $\Phi(x)\rightarrow t$. At the boundary of $x=0$, both $\Psi(x)$ and $d\Psi/dx$ must be continuous. We denote r as the reflection amplitude, and normalize the incoming wave to 1, then the reflectivity is given by

$$ R=|r|^2 , \tag{27} $$

and the boundary conditions at $x=0$ then become

$$ 1+r=t\,{}_0F_1(1-2i\kappa\lambda;\lambda^2u_M) \tag{28} $$

and

$$ ik_x(1-r)=i\kappa t\,{}_0F_1(1-2i\kappa\lambda;\lambda^2u_M) $$

$$ -\frac{\lambda^2u_M}{\lambda(1-2i\kappa\lambda)}t\,{}_0F_1(2-2i\kappa\lambda;\lambda^2u_M) . \tag{29} $$

Solving r and t from Eqs. (28) and (29) we obtain

$$ r=\frac{(k_x-\kappa)\lambda(1-2i\kappa\lambda){}_0F_1(1-2i\kappa\lambda;\lambda^2u_M)-i\lambda^2u_M{}_0F_1(2-2i\kappa\lambda;\lambda^2u_M)}{(k_x+\kappa)\lambda(1-2i\kappa\lambda){}_0F_1(1-2i\kappa\lambda;\lambda^2u_M)+i\lambda^2u_M{}_0F_1(2-2i\kappa\lambda;\lambda^2u_M)} , \tag{30a} $$

$$ t=\frac{2k_x\lambda(1-2i\kappa\lambda)}{(k_x+\kappa)\lambda(1-2i\kappa\lambda){}_0F_1(1-2i\kappa\lambda;\lambda^2u_M)+i\lambda^2u_M{}_0F_1(2-2i\kappa\lambda;\lambda^2u_M)} , \tag{30b} $$

and, finally, the reflectivity

$$ R=\left|\frac{(k_x-\kappa)\lambda(1-2i\kappa\lambda){}_0F_1(1-2i\kappa\lambda;\lambda^2u_M)-i\lambda^2u_M{}_0F_1(2-2i\kappa\lambda;\lambda^2u_M)}{(k_x+\kappa)\lambda(1-2i\kappa\lambda){}_0F_1(1-2i\kappa\lambda;\lambda^2u_M)+i\lambda^2u_M{}_0F_1(2-2i\kappa\lambda;\lambda^2u_M)}\right|^2 . \tag{31} $$

We note that since $k_x=(2\pi/\lambda_n)\sin\theta$, where λ_n is the neutron's wavelength, the reflectivity R can be regarded as a function of λ_n for a fixed incident angle θ, or as a function of θ for a selected wavelength. The former is most appropriate for pulsed neutron sources, while the latter is the practice at reactor-type neutron sources. As our particular interest is reflectivity measurements at a fixed wavelength we will choose θ as the independent variable in the following discussions.

III. DISCUSSION OF THE SOLUTION FOR $R^{\pm}(\theta,\lambda)$

A. General behavior

First we set the external magnetic field to zero ($u_M=0$), so that the reflectivity [Eq. (31)] reduces to

$$ R=\left|\frac{k_x-\kappa}{k_x+\kappa}\right|^2 , \tag{32} $$

which is the familiar textbook solution of the 1D Schrödinger equation with a simple step potential. Note that $R=1$ [Eq. (32)] when $k_x\leq u_N^{1/2}$, so $k_{xc}=k\sin\theta_c=u_N^{1/2}$ defines the critical angle for total reflection, as in Eq. (2) with $p=0$.

Now we take the case when the external magnetic field H is nonzero, but below H_{c1}, so that the sample is in its Meissner state; H is typically on the order of a few hundred oersteds or less. The region of total reflection ($R=1$) becomes $k_x\leq(u_N-u_M)^{1/2}$. To see this we note from Eq. (16) that κ is now pure imaginary in this regime, so we may write $\kappa=i\tilde{\kappa}$ where $\tilde{\kappa}$ is real and $\tilde{\kappa}\geq 0$. Then the reflectivity [Eq. (31)] can be simplified as

$$ R=\left|\frac{A-iB}{A+iB}\right|^2 , \tag{33} $$

where

$$ A\equiv k_x\lambda(1+2\tilde{\kappa}\lambda){}_0F_1(1+2\tilde{\kappa}\lambda;\lambda^2u_M) \tag{34} $$

and

$$ B\equiv\tilde{\kappa}\lambda(1+2\tilde{\kappa}\lambda){}_0F_1(1+2\lambda\tilde{\kappa};\lambda^2u_M) $$

$$ +\lambda^2u_M{}_0F_1(2+2\tilde{\kappa}\lambda;\lambda^2u_M) . \tag{35} $$

Since A and B are both real functions, $R=1$. However, defining $k_{xc}=k\sin\theta_c=(u_N-u_M)^{1/2}$, the critical angle is now spin dependent, since u_M is spin dependent [Eq. (11)]. Hence we have two different critical angles for spin-up ($+$) and spin-down ($-$) neutrons, respectively:

$$ \theta_c^{\pm}\equiv\sin^{-1}\left[(u_N\mp|u_M|)^{1/2}\frac{\lambda_n}{2\pi}\right] . \tag{36} $$

Note that $\theta_c^->\theta_c^+$. If we take $\lambda_n=2.35$ Å, $H=500$ Oe, and $u_N=4.98\times10^{-5}$ Å^{-2} appropriate for niobium, the critical angles are $\theta_c^+=0.1489°$ and $\theta_c^-=0.1533°$, and the critical angle splitting is $(\theta_c^--\theta_c^+)=0.0044°$. As θ^- and θ^+ are small for thermal or cold neutrons, the critical angle splitting for spin-up and spin-down neutrons can be

written as

$$\theta_c^- - \theta_c^+ = \frac{\lambda_n |u_M|}{2\pi u_N^{1/2}} = \frac{c}{\pi^{1/2}} \frac{\lambda_n H_0}{(Nb)^{1/2}} , \tag{37}$$

so $(\theta_c^- - \theta_c^+)$ is proportional to the neutron's wavelength λ_n as well as the applied magnetic field H.

Figure 2 shows $R^+(\theta)$ (dash-dot curve) and $R^-(\theta)$ (solid curve) for three different choices of the penetration depth λ: (a) 400 Å, (b) 1000 Å, and (c) 1600 Å, with $\lambda_n = 2.35$ Å, $H = 500$ Oe, and $u_N = 4.98 \times 10^{-5}$ Å^{-2}. The double-dot-dashed line is the reflectivity for $H = 0$. First consider the curves for $R^+(\theta)$. As θ exceeds θ_c^+, $R^+(\theta)$ decreases monotonically, and the larger λ is, the slower $R^+(\theta)$ decreases above θ_c^+. This is the type of behavior expected based on previous (numerical) results.

The behavior of $R^-(\theta)$, on the other hand, is surprising, as it does not always decrease monotonically as a function of θ above θ_c^-. For example, at $\lambda = 1000$ Å, $R^-(\theta)$ almost dips to zero immediately above θ_c^- [Fig. 2(b)]. In other words, there is nearly total transmission. Beyond this dip, $R^-(\theta)$ is slightly above $R^+(\theta)$, reflecting the fact that the asymptotic value of $u^-(x)$ is above that of $u^+(x)$ by $2|u_M|$ (Fig. 1). As θ continues to increase, $R^-(\theta)$ and $R^+(\theta)$ merge into one curve as $2|u_M|$ becomes small compared to the kinetic energy term controlled by $k_x = k \sin\theta$. Thus these spin-dependent effects are most discernible in the vicinity of the critical angles.

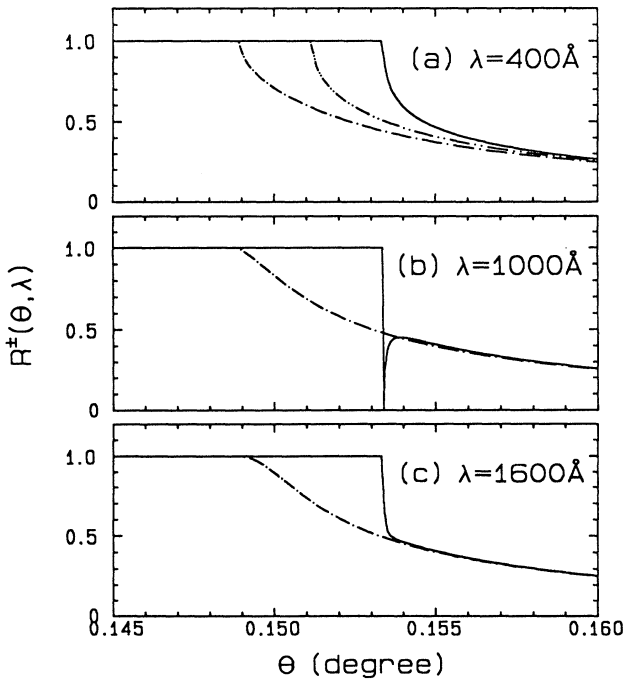

FIG. 2. Reflectivity calculated from Eq. (31) for spin-up $[R^+(\theta,\lambda)$ (dash-dot curves)] and spin-down $[R^-(\theta,\lambda)$ (solid curves)] neutrons, as a function of θ, for three different values of the magnetic penetration depth λ. Parameters used for plotting are $\lambda_n = 2.35$ Å, $H = 500$ Oe, and $u_N = 4.98 \times 10^{-5}$ Å^{-2} (for niobium). $\lambda = 400$ Å (a), 1000 Å (b), and 1600 Å (c). The double-dot-dashed line in (a) is the reflectivity for $H = 0$.

B. Anomalous resonant transmission in $R^-(\theta,\lambda)$

The "dip" in the reflectivity profile for spin-down neutrons shown in Fig. 2(b) was an unexpected feature revealed by the analytical expression for $R(\theta,\lambda)$. In actual reflectivity measurements from thin films we typically see oscillatory behavior in $R(\theta)$ due to interference from the waves scattered from the front and back surfaces of the sample. In the present case, however, the sample is assumed to be infinitely thick and hence this structure in $R^-(\theta)$ must have a different origin. This phenomenon appears to be related to the scattering potential, as we have not seen it discussed in other 1D quantum-mechanical scattering problems in the literature. This λ-dependent resonance effect is worth studying because it has the potential to be developed into a sensitive way to measure λ. In the following paragraphs we first give some intuitive physical arguments as to the origin of this anomalous transmission effect. We also demonstrate that the reflectivity coefficient given by Eq. (31) can indeed vanish, and we derive the resonant conditions for H and λ. We then present a simplified calculation which demonstrates the essential physics behind this anomalous resonant transmission, and finally discuss a possible way to experimentally detect the effect.

To get an understanding of how this resonant transmission may happen, let us do the calculation as it would be done numerically, that is, we divide the sample into thin layers and assign to each layer the appropriate average scattering potential. Then the scattering potential for spin-down neutrons shown in Fig. 1(b) is transformed to a stair potential as shown in Fig. 3. If we let the incoming neutron's energy be higher than the asymptotic value of the potential, then at each interface, as well as the front surface, the neutron wave is partially reflected and partially transmitted. If the waves reflected from all the interfaces happen to have the correct phases and amplitudes so that they add up destructively in the $x < 0$ region, then we might, in principle, have a suppressed reflectivity, or even have $r = 0$ where the neutron wave would be totally transmitted. The phase and amplitude of the reflected wave from each interface depends on both the potential difference between the two adjacent layers as well as the distance from the interface to the front surface. As the layer thickness approaches zero, this means

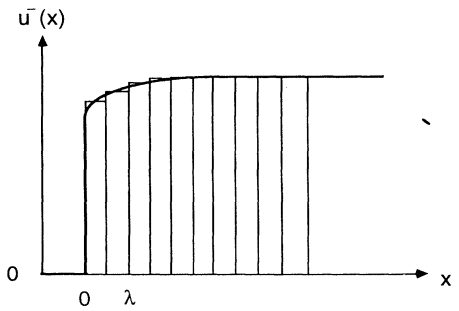

FIG. 3. Stair potential as an approximation to $u(x)$ for spin-down neutrons.

that the potential curve would have to have a specific shape and magnitude in order to produce such destructive interference, and we will find that H and λ need to satisfy certain stringent conditions in order for this effect to occur.

To study the anomalous resonant transmission analytically, let us consider Eq. (31) in the κ range where

$$0<\kappa\lambda\ll 1 \ . \tag{38}$$

For the magnetic-field range we are considering and for most materials Eq. (38) guarantees that

$$0<\frac{\kappa}{k_{xc}}\ll 1 \ , \tag{39}$$

where

$$k_{xc}\equiv(u_N-u_M)^{1/2} \tag{40}$$

because $k_{xc}\lambda>1$. For example, for $u_N=4.98\times10^{-5}$ Å^{-2}, $H=500$ Oe, and $\lambda=300$ Å we have $k_{xc}\lambda=2.1>1$. We therefore expand both the numerator and the denominator of r in Eq. (30) to first order in $\kappa\lambda$ and κ/k_{xc}. Using

$$k_x=(k_{xc}^2+\kappa^2)^{1/2}=k_{xc}+O(\kappa^2/k_{xc}^2) \ , \tag{41a}$$

$$(k_x\mp\kappa)\lambda(1-2i\kappa\lambda)=k_{xc}\lambda-(\pm1+2ik_{xc}\lambda)\kappa\lambda+O(\kappa^2\lambda^2) \ , \tag{41b}$$

$${}_0F_1(1-2i\kappa\lambda;\lambda^2u_M)={}_0F_1(1;\lambda^2u_M)-2i\,{}_0F'_{1,1}(1;\lambda^2u_M)\kappa\lambda+O(\kappa^2\lambda^2) \ , \tag{41c}$$

$${}_0F_1(2-2i\kappa\lambda;\lambda^2u_M)={}_0F_1(2;\lambda^2u_M)-2i\,{}_0F'_{1,1}(2;\lambda^2u_M)\kappa\lambda+O(\kappa^2\lambda^2) \ , \tag{41d}$$

and neglecting terms $\sim O(\kappa^2/k_{xc}^2)$ or $\sim O(\kappa^2\lambda^2)$, we find that Eq. (30a) can be written in a simpler form:

$$r\cong\frac{(f_1+if_2)-(f_3+if_4)\kappa\lambda}{(f_1-if_2)+(f_3-if_4)\kappa\lambda} \ , \tag{42}$$

where f_1, f_2, f_3, and f_4 are real functions defined by

$$f_1\equiv k_{xc}\lambda\,{}_0F_1(1;\lambda^2u_M) \ , \tag{43a}$$

$$f_2\equiv-\lambda^2u_M\,{}_0F_1(2;\lambda^2u_M) \ , \tag{43b}$$

$$f_3\equiv{}_0F_1(1;\lambda^2u_M)+2\lambda^2u_M\,{}_0F'_{1,1}(2;\lambda^2u_M) \ , \tag{43c}$$

$$f_4\equiv2k_{xc}\lambda[{}_0F_1(1;\lambda^2u_M)+{}_0F'_{1,1}(1;\lambda^2u_M)] \ . \tag{43d}$$

These four dimensionless functions are independent of θ and the neutron wavelength λ_n. Rather, they are determined only by the shape and magnitude of the potential through parameters such as u_N, u_M, and λ. We remark that the ${}_0F_1$ functions in Eqs. (43) may be replaced by Bessel functions via Eqs. (25), and noting that $J_n(z)$ is oscillatory while $I_n(z)$ is monotonic we may anticipate an oscillatory dependence of r on λ for spin-down neutrons ($u_M<0$), and thus the possibility of total transmission.

In the κ range specified by Eq. (38) the reflectivity becomes

$$R\cong\frac{(f_1-f_3\kappa\lambda)^2+(f_2-f_4\kappa\lambda)^2}{(f_1+f_3\kappa\lambda)^2+(f_2+f_4\kappa\lambda)^2} \ . \tag{44}$$

Hence a sufficient condition for a total transmission to occur is given by the following two equations:

$$f_1=f_3\kappa\lambda \ , \tag{45}$$

$$f_2=f_4\kappa\lambda \ , \tag{46}$$

together with Eq. (38). Eliminating $\kappa\lambda$ we find

$$0<\frac{f_1}{f_3}=\frac{f_2}{f_4}\ll1 \ . \tag{47}$$

From the above equation we see that it is the shape of the potential curve that determines whether this total transmission may happen, independent of the wave vector k_x or angle θ. The value of k_x (and θ) at which this total transmission will occur can be calculated from the result of Eq. (47) by using $\kappa\lambda=f_1/f_3$, or more explicitly

$$k_x^2=\left[\frac{f_1}{f_3\lambda}\right]^2+u_N-u_M \ . \tag{48}$$

We may use a graphical method to obtain the solutions of Eq. (47). Figure 4 is a plot of f_1/f_3 and f_2/f_4 as a function of λ for spin-down neutrons, again using $H=500$ Oe and $u_N=4.98\times10^{-5}$ Å^{-2}. The dash-dot curve represents f_1/f_3, while the solid line is f_2/f_4; they do indeed cross, and several crossing points have values positive and much smaller than 1. We tabulate the first four such crossings in Table I.

We may also obtain an approximate expression for the solutions by noting in Fig. 4 that f_1/f_3 is not as flat as f_2/f_4 at the intersections tabulated in Table I. Therefore, Eq. (47) can be approximated by

$$\frac{f_1}{f_3}\cong0 \tag{49}$$

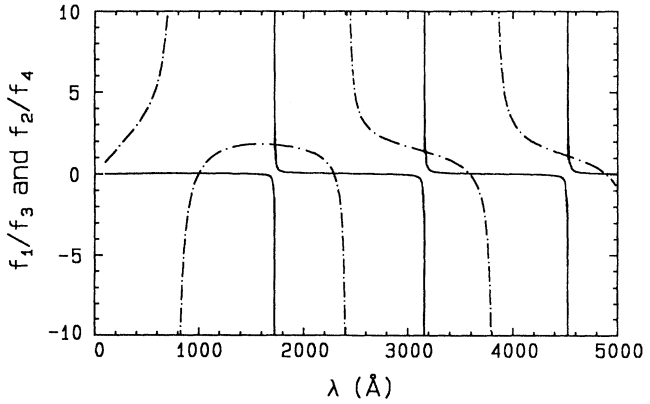

FIG. 4. Plot of the dimensionless functions f_1/f_3 (dash-dot line) and f_2/f_4 (solid line). Parameters λ_n, H, and u_N used are the same as those in Fig. 2. The intersections which have values much smaller than 1 yield solutions of λ at which total transmission occurs. Four such crossings are in the plot. These λ's and the corresponding functional values are listed in Table I.

TABLE I. Solutions of Eq. (47).

λ	$f_1/f_3=f_2/f_4$
1002.326	0.0545
2287.469	0.0540
3584.076	0.0544
4883.646	0.0548

or simply $f_1 \cong 0$. From Eq. (43a) we get

$$ {}_0F_1(1;\lambda^2 u_M) \cong 0 \ . \tag{50}$$

For spin-down neutrons $u_M < 0$, so from Eq. (25b) we have

$$ {}_0F_1(1;\lambda^2 u_M) = J_0(2\lambda |u_M|^{1/2}) \ . \tag{51}$$

Hence the condition for the total transmission becomes

$$ J_0[2\lambda(4\pi c H)^{1/2}] \cong 0 \ , \tag{52}$$

so that to a good approximation $2\lambda(4\pi c H)^{1/2}$ needs to be a root of the zeroth-order Bessel function:

$$ 2\lambda(4\pi c H)^{1/2} \cong 2.4048,\ 5.5201,\ 8.6537,\ 11.7915\ , \cdots \ . \tag{53}$$

We emphasize that here it is the shape of the potential curve that determines whether total transmission may occur.

A better understanding of the physical origin of this potential-profile-dependent, single-dip resonant transmission may be obtained by examining a much simpler potential profile which consists of only two steps:

$$ u(x) = \begin{cases} 0 \ , & x < 0 \\ u_1 \ , & 0 \le x < a \\ u_2 \ , & x \ge a \end{cases} \tag{54}$$

as shown in Fig. 5. Define

$$ \kappa_1 \equiv +(k_x^2 - u_1)^{1/2} \tag{55}$$

and

$$ \kappa_2 \equiv +(k_x^2 - u_2)^{1/2} \ . \tag{56}$$

The reflectivity can be calculated in the usual way by solving the Schrödinger equation in the three regions and matching the boundary conditions. The results are

$$ r = \frac{(k_x-\kappa_1)(\kappa_1+\kappa_2)+(\kappa_1-\kappa_2)(k_x+\kappa_1)\exp(2i\kappa_1 a)}{(k_x+\kappa_1)(\kappa_1+\kappa_2)+(\kappa_1-\kappa_2)(k_x-\kappa_1)\exp(2i\kappa_1 a)} \tag{57}$$

and

$$ R = |r|^2 = \frac{\kappa_1^2(k_x-\kappa_2)^2\cos^2(\kappa_1 a)+(\kappa_1^2-k_x\kappa_2)^2\sin^2(\kappa_1 a)}{\kappa_1^2(k_x+\kappa_2)^2\cos^2(\kappa_1 a)+(\kappa_1^2+k_x\kappa_2)^2\sin^2(\kappa_1 a)} \ . \tag{58}$$

Taking $k_x^2 > u_1$ and $k_x^2 > u_2$, we have two sets of conditions for total transmission ($R=0$):

$$ \begin{cases} k_x = \kappa_2 \\ \kappa_1 a = n\pi \ , \quad n = 0,1,2,\ldots \end{cases} \tag{59}$$

or

$$ \begin{cases} \kappa_1^2 = k_x \kappa_2 \\ \kappa_1 a = (n+\frac{1}{2})\pi \ , \quad n = 0,1,2,\ldots \ . \end{cases} \tag{60}$$

The first set implies

$$ \begin{cases} u_2 = 0 \\ k_x^2 = u_1 + (n\pi/a)^2 \ , \quad n = 0,1,2,\ldots \ , \end{cases} \tag{61}$$

which is the ordinary resonant transmission for a square-potential barrier. Notice that Eq. (61) does not put any constraints on u_1 or a. In particular, there is no constraint on the sign of u_1, i.e., whether it is repulsive or attractive. As θ (and k_x) varies, the resonance condition is met periodically. This is the k_x-dependent resonance we usually see, as in the reflectivity from a thin film. The second set of conditions can be rewritten as

$$ a\left[\frac{(u_2-u_1)u_1}{2u_1-u_2}\right]^{1/2} = (n+\tfrac{1}{2})\pi \ , \quad n = 0,1,2,\ldots \tag{62}$$

and

$$ k_x = \frac{u_1}{(2u_1-u_2)^{1/2}} \ . \tag{63}$$

Notice that Eq. (62) is a condition on the shape of the potential, independent of k_x. The total transmission effect occurs only when

$$ u_1 < u_2 < 2u_1 \tag{64}$$

and the first potential step has the correct width a, and only at a specific value of k_x given by Eq. (63). Hence there is only a single dip in $R(\theta)$.

The physics behind these two sets of resonance conditions [Eqs. (59) and Eqs. (60)] has a simple and unified scheme: Total transmission occurs when the waves reflected from the front surface $x=0$ and the interface $x=a$ add up completely destructively in the $x<0$ region, or in other words, when they have equal amplitudes but opposite phase. Let us consider the square potential first. Since the potential jumps at $x=0$ and $x=a$ are equal in absolute value but differ by a sign, the two reflected

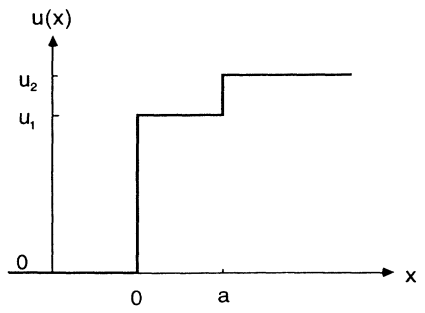

FIG. 5. The two-step potential defined in Eq. (54).

waves have the same amplitude but are out of phase. Thus the extra phase change of the wave reflected from $x=a$, due to traveling a longer distance $2a$, must equal $2n\pi$, i.e., $\kappa_1(2a)=2n\pi$. This is the resonance condition Eq. (59). In the second case, when $u_2>u_1$, the potential jumps at $x=0$, and $x=a$ have the same sign, so there is no phase change upon being reflected, and thus the phase change due to travelling a longer distance $2a$ must be $(2n+1)\pi$, i.e., $\kappa_1(2a)=(2n+1)\pi$. This is the second half of the resonance condition Eq. (60). The equal amplitude condition requires, in reference to Eq. (32), that

$$\frac{k_x-\kappa_1}{k_x+\kappa_1}=\frac{\kappa_1-\kappa_2}{\kappa_1+\kappa_2}\ , \tag{65}$$

which gives $\kappa_1^2=k_x\kappa_2$, the first half of the resonance condition Eq. (60). In summary, there are two types of resonant transmission: the conventional *k_x-oscillatory type*, and the *potential-profile-dependent* and *single-dip* type. Both have the same physical origin—the reflected waves add up destructively.

C. Possible detection of the anomalous transmission with ultracold neutrons

We return to Eq. (48) to determine the angular difference between the total transmission angle θ_{tt}, and the critical angle θ_c^-. From Eq. (48) we have

$$k_x^2-k_{xc}^2=\left[\frac{f_1}{f_3\lambda}\right]^2 . \tag{66}$$

When the total transmission condition [Eq. (47)] is met, f_1/f_3 is much smaller than 1, and therefore the right-hand side of Eq. (66) is very small and θ_{tt} is very close to θ_c^-. Then Eq. (66) can be rewritten as

$$\sin\theta_{tt}-\sin\theta_c^-=\frac{\lambda_n}{4\pi k_{xc}}\left[\frac{f_1}{f_3\lambda}\right]^2 , \tag{67}$$

where we note that the right-hand side is proportional to the neutron wavelength. Taking $H=500$ Oe, $u_N=4.98\times10^{-5}$ Å^{-2}, and $\lambda\cong1002$ Å, where the first total transmission occurs (Table I), we have $f_1/f_3\cong0.0545$ and $k_{xc}=(u_N+|u_M|)^{1/2}=0.007\,15$ Å^{-1}, which gives

$$\sin\theta_{tt}-\sin\theta_c^-=3.3\times10^{-8}\lambda_n \tag{68}$$

or

$$\theta_{tt}-\theta_c^-=(2\times10^{-6}/\cos\theta_c^-)\lambda_n\ , \tag{69}$$

where the angle is in degrees. The very cold to ultracold neutron regime will make this angular difference easier to resolve experimentally. The resonance condition may be tuned by varying the magnetic penetration depth (with temperature) or by varying the applied field.

D. Oscillatory dependence of $R^-(\theta,\lambda)$ on λ

Since the occurrence of the total transmission depends on λ quasiperiodically, as indicated in Eq. (53), the λ dependence of $R^-(\theta,\lambda)$ at $\theta\gtrsim\theta_c$ must also be quasiperiodic. Figure 6 plots $R^-(\theta,\lambda)$ (solid line) as a function of λ at three different values of θ. The dash-dot lines are $R^+(\theta,\lambda)$ plotted just for comparison, and again we have taken $\lambda_n=2.35$ Å, $H=500$ Oe, and $u_N=4.98\times10^{-5}$ Å^{-2}. At $\theta=0.1534°$ [Fig. 6(a)], $R^-(\theta,\lambda)$ clearly shows an oscillatory dependence on λ. At $\theta=0.1550°$, on the other hand, $R^-(\theta,\lambda)$ is monotonic. This is less than 0.002° from θ_c^- (0.1533°), which is beyond the angular resolution available currently.[2,3,12]

E. Thick-film case

The above analytic results have been for a superconducting system which is assumed infinite in thickness, and the question naturally arises whether these effects survive and might be observable in actual materials. We have therefore investigated the analytic expression of the reflectivity from a thick superconducting film. In the case of a free-standing film with identical surfaces on both sides, the reflectivity $\tilde{R}^{\pm}(\theta,\lambda)$ is simply related to $R^{\pm}(\theta,\lambda)$ by

$$\tilde{R}^{\pm}(\theta,\lambda)=\frac{2R^{\pm}(\theta,\lambda)}{1+R^{\pm}(\theta,\lambda)} \tag{70}$$

provided that the thickness of the film, d, is so large that $d\gg\lambda$ and the oscillatory terms in $\tilde{R}^{\pm}$ due to the film thickness are averaged, which is practical due to finite instrumental resolution. We will prove this result in Sec. III. From Eq. (70) we observe that all the interesting features of $R^-(\theta,\lambda)$—the dip, the total transmission,

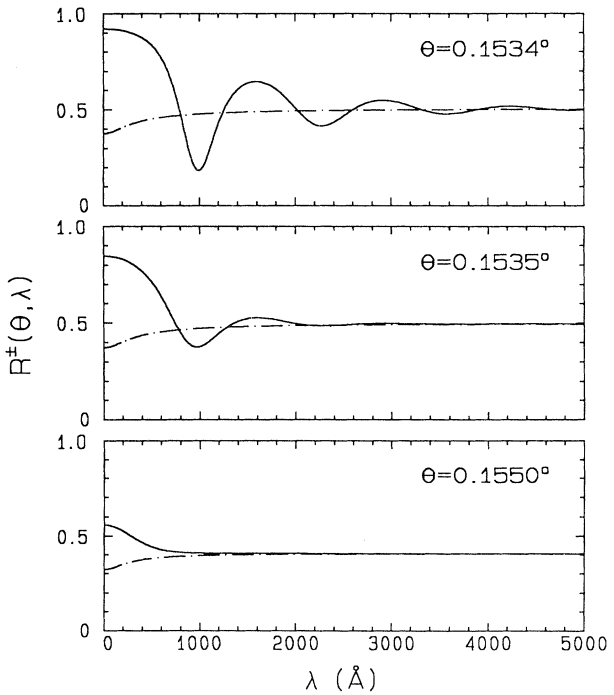

FIG. 6. Reflectivity calculated from Eq. (31) for spin-up [$R^+(\theta,\lambda)$ (dash-dot curves)] and spin-down [$R^-(\theta,\lambda)$ (solid curves)] neutrons, as a function of λ, for three different values of θ. The parameters λ_n, H, and u_N used are the same as those in Fig. 2. $\theta=0.1534°$ (a), 0.1535° (b), and 0.1550° (c).

and the oscillatory dependence on λ—persist in $\tilde{R}^{-}(\theta,\lambda)$, and therefore no information is lost in using a thick film. Indeed, from a practical point of view use of a thick film allows one to measure the transmission coefficient $\tilde{T}^{\pm}(\theta,\lambda)=1-\tilde{R}^{\pm}(\theta,\lambda)$. The advantage is that the anomalous peak in $\tilde{T}^{-}(\theta,\lambda)$ [corresponding to the dip in $\tilde{R}^{-}(\theta,\lambda)$] arises sharply from *zero* when θ increases above θ_c^{-}, and hence this may provide a superior signal-to-background ratio.

IV. $\tilde{R}^{\pm}(\theta,\lambda)$ FOR A THICK FILM

When we consider a sample of finite thickness, we have to consider multiple reflections between the two boundaries, allowing the amplitude of the reflected and transmitted wave to change on each "bounce". Fortunately, the multiple reflections of the incoming wave compose a geometric series[15] which may be easily handled mathematically, and the sum of the series is the resultant reflectivity we desire.

To demonstrate the principle of this method, let us rederive the reflectivity of the two-step potential (Fig. 5), which we obtained earlier [Eq. (54)] as an exact solution of the Schrödinger equation by matching boundary conditions. Define κ_1 as in Eq. (55) and κ_2 as in Eq. (56), and let (r_1,t_1), (r_2,t_2), and (r_3,t_3) be the reflection and transmission amplitudes for single interfaces, with the x-axis origin defined as in Fig. 7(a) and Fig. 7(b), respectively. Then the multiple reflection diagram can be schematically shown as in Fig. 7(c). Summing up all the reflections on the $x<0$ side, we have

$$r=r_1+t_1r_3t_2\exp(2i\kappa_1a)\sum_{n=0}^{+\infty}[r_2r_3\exp(2i\kappa_1a)]^n$$
$$=\frac{r_1+(t_1t_2-r_1r_2)r_3\exp(2i\kappa_1a)}{1-r_2r_3\exp(2i\kappa_1a)} . \quad (71)$$

We know that

$$r_1=\frac{k_x-\kappa_1}{k_x+\kappa_1} , \quad t_1=\frac{2k_x}{k_x+\kappa_1} , \quad (72a)$$

$$r_2=\frac{\kappa_1-k_x}{\kappa_1+k_x} , \quad t_2=\frac{2\kappa_1}{\kappa_1+k_x} , \quad (72b)$$

$$r_3=\frac{\kappa_1-\kappa_2}{\kappa_1+\kappa_2} , \quad t_3=\frac{2\kappa_1}{\kappa_1+\kappa_2} . \quad (72c)$$

We can rearrange them to obtain

$$r_2=-r_1 , \quad (73a)$$

$$t_1t_2-r_1r_2=1 , \quad (73b)$$

and finally

$$r=\frac{r_1+r_3\exp(2i\kappa_1a)}{1+r_1r_3\exp(2i\kappa_1a)}$$
$$=\frac{(k_x-\kappa_1)(\kappa_1+\kappa_2)+(\kappa_1-\kappa_2)(k_x+\kappa_1)\exp(2i\kappa_1a)}{(k_x+\kappa_1)(\kappa_1+\kappa_2)+(\kappa_1-\kappa_2)(k_x-\kappa_1)\exp(2i\kappa_1a)} , \quad (74)$$

which is identical to Eq. (57).

There are two points we would like to make about this method. First, if we know the reflection and transmission amplitudes at the separate boundaries, we can construct the reflection (and similarly transmission) amplitude for the composite structure by summing up all the multiple reflections, provided that between the boundaries there exists only a constant potential and hence a plane-wave solution. Secondly, (r_2,t_2) is the time-reversal solution of (r_1,t_1) and therefore is not independent of (r_1,t_1), and in fact they can be eliminated from the final expression.

This geometric series method of calculating reflectivity can be extended to the case where two boundary

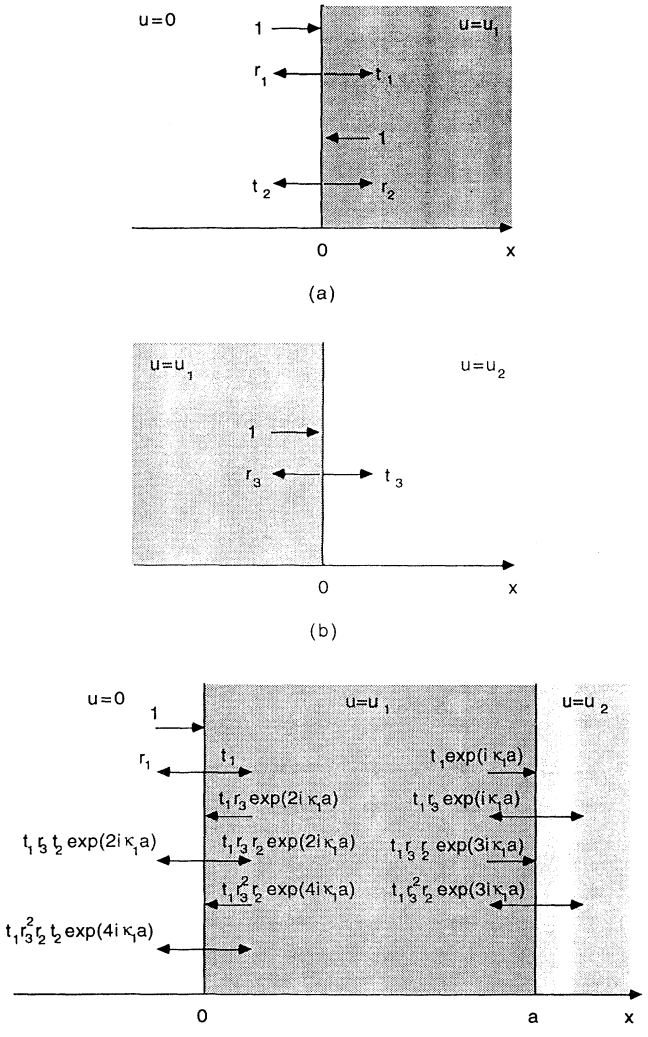

FIG. 7. Reflection and transmission of a plane wave at the first (a) and second (b) boundary, and the schematic diagram of multiple reflections (c). (r_1,t_1), (r_2,t_2), and (r_3,t_3) are the reflection and transmission amplitudes obtained with respect to the x-axis origin chosen as in (a) and (b). In (c) the reflection amplitues on the $x<0$ side compose a geometric series and the sum of the series is identical to the exact solution. The attenuation factor of the series is $r_2r_3\exp(2i\kappa_1a)$ due to "bouncing" once from each boundary and traveling a distance $2a$ with a wave vector κ_1.

"blocks" are connected by a constant potential, in contract to two boundary "planes" in the previous example. The boundary blocks can be treated like black boxes which may consist of complicated layered structures such as a multilayer or an exponential change in scattering potential, etc. All we need to know about these "black-box" blocks is their reflection and transmission amplitudes. We assume that the reflection and transmission amplitudes of the boundary blocks are known by other means and given *a priori*, and use them to express the resultant reflectivity of the composite structure. Figure 8 shows two such boundary blocks. L_1 and L_2 indicate block thickness. We do not have to be concerned about the details of the potential functions $u(x)$ and $u'(x)$ for the time being as long as we know that (r_1,t_1) and (r_3,t_3) are obtained with respect to the x-axis origin chosen as in Fig. 8(a) and Fig. 8(b), respectively, and these amplitudes are indeed known *a priori*. The multiple reflection diagram then is shown as in Fig. 9. We denote the film thickness L_1+a+L_2 by d and find that after the second reflection the attenuation factor for each subsequent reflection on the $x<0$ side is $r_2r_3\exp(2i\kappa_1 d)$. We thus have

$$r=r_1+t_1r_3t_2\exp(2i\kappa_1 d)\sum_{n=0}^{+\infty}[r_2r_3\exp(2i\kappa_1 d)]^n$$
$$=\frac{r_1+(t_1t_2-r_1r_2)r_3\exp(2i\kappa_1 d)}{1-r_2r_3\exp(2i\kappa_1 d)} . \tag{75}$$

Since (r_1,t_1) and (r_2,t_2) are not independent of each other, we can express them as two independent variables (α,β):[16]

$$r_1=-\frac{\beta^*}{\alpha^*} , \tag{76a}$$

$$t_1=\frac{1}{\alpha^*}(|\alpha|^2-|\beta|^2) , \tag{76b}$$

$$r_2=\frac{\beta}{\alpha^*} , \tag{76c}$$

$$t_2=\frac{1}{\alpha^*} . \tag{76d}$$

Then we have

$$t_1t_2-r_1r_2=\frac{\alpha}{\alpha^*} . \tag{77}$$

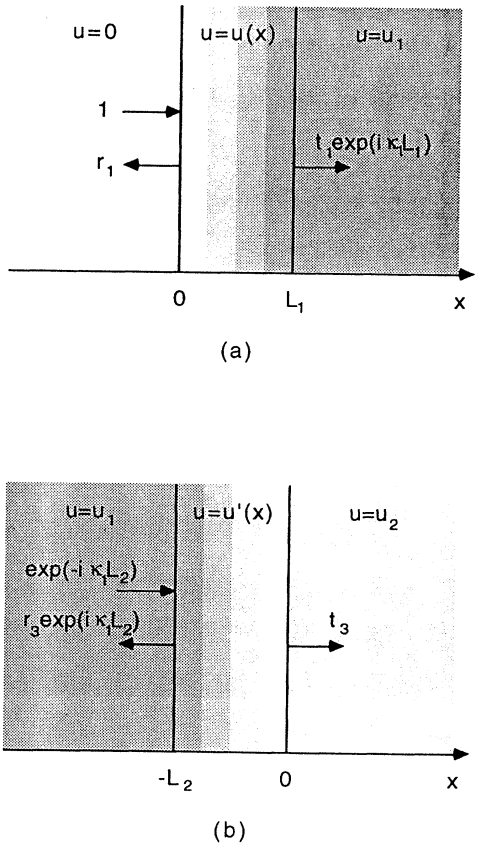

FIG. 8. Reflection and transmisson of a plane wave at the first (a) and the second (b) boundary blocks, rather than boundary planes. (r_1,t_1) and (r_3,t_3) are the reflection and transmission amplitudes obtained with respect to the x-axis origin chosen as in (a) and (b). Constant potentials and plane wave solutions are assumed outside the blocks.

Defining the real number φ as $\exp(i\varphi)=\alpha/\alpha^*$, we have

$$r=\frac{r_1+r_3\exp(2i\kappa_1 d+i\varphi)}{1+r_1^*r_3\exp(2i\kappa_1 d+i\varphi)} \tag{78}$$

and

$$|r|^2=\frac{|r_1|^2+|r_3|^2+2\,\mathrm{Re}\{r_1^*r_3\}\cos(\kappa_1 d+\varphi/2)-2\,\mathrm{Im}\{r_1^*r_3\}\sin(\kappa_1 d+\varphi/2)}{1+|r_1|^2|r_3|^2+2\,\mathrm{Re}\{r_1^*r_3\}\cos(\kappa_1 d+\varphi/2)-2\,\mathrm{Im}\{r_1^*r_3\}\sin(\kappa_1 d+\varphi/2)} . \tag{79}$$

This equation is an exact result and may have various applications in reflectivity calculations. Our superconducting film case, which we will discuss shortly, is only a special example. Another example is the two-step potential including interfacial roughness. The interfacial roughness is commonly modeled by a smooth function connecting the two constant potentials, for example error function or hyperbolic tangent function (or equivalently a Fermi function). The error function has been very popular because in the kinematic limit the reflectivity is simply related to the Fourier transform of the potential's first derivative and the error function's first derivative is the Gaussian function, and its Fourier transform is simple to handle. Now in view of Eq. (79), the hyperbolic tangent

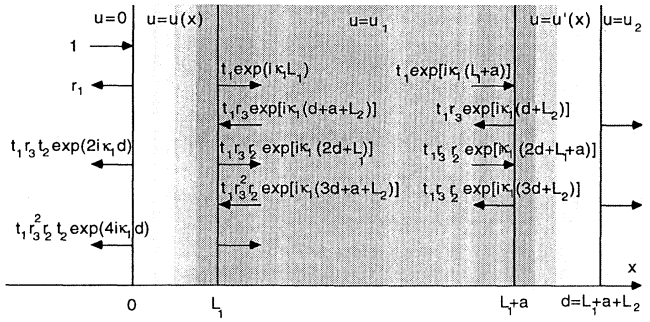

FIG. 9. Schematic diagram of multiple reflections from two boundary blocks. The attenuation factor for the multiple reflections on the $x<0$ side is $r_1 r_3 \exp(2i\kappa_1 d)$, where $d=L_1+a+L_2$ is the thickness of the film.

function is very useful because the exact solution of the Schrödinger equation with a hyperbolic tangent potential is known.[16] Therefore, we may have a simple analytic expression for the reflectivity for the smeared-two-step potential, which is valid not only in the kinematic limit but throughout the total reflection region. Moreover, the geometric series method can be extended to many black-box blocks rather than being limited by two when it is applied recursively. For example, it is readily applicable to multilayer systems with interfacial roughness.

Now let us consider Eq. (79) in the thick-film limit. When d in Eq. (79) is very large the oscillatory terms vary rapidly with angle θ, and over the finite angular acceptance of the reflectometer instrumental resolution the reflectivity is averaged to[17]

$$R=\frac{R_1+R_3-2R_1R_3}{1-R_1R_3} . \tag{80}$$

To apply this general formula to our thick superconducting film case, we first examine our boundary blocks. For the first block, when $L_1 \gg \lambda$, the transmission amplitude becomes [Eq. (24) and Eq. (30b)]

$$t_0 F_1[1-2i\kappa\lambda;\lambda^2 u_M \exp(-L_1/\lambda)] = t[1+O(\exp(-L_1/\lambda))] , \tag{81}$$

so we can safely replace it by t itself in the thick-film limit. In this manner we have successfully constructed our first boundary block. Taking the second boundary block as the mirror image of the first, we find that

$$\tilde{R}^{\pm}(\theta,\lambda)=\frac{2R^{\pm}(\theta,\lambda)}{1+R^{\pm}(\theta,\lambda)} \tag{82}$$

for a free-standing thick superconducting film.

If the film is grown on a substrate, we can still use the exact solution $R^{\pm}(\theta,\lambda)$ to express R_3, and the only change is in u_N. However, the total transmission for the two boundary blocks does not occur at the same angle θ because θ_c^- (and hence θ_{tt}) are quite different. We emphasize that the mirror symmetry of the film and the surface quality are important if the anomalous transmission is to be observed experimentally.

V. OTHER APPLICATIONS OF $R^{\pm}(\theta,\lambda)$ AND $\tilde{R}^{\pm}(\theta,\lambda)$

Even though we have limited our detailed discussions to the magnetic penetration depth λ in superconductors, the exact solution[18] $R^{\pm}(\theta,\lambda)$ can be applied to other systems where the scattering potential has an exponential dependence with distance in the surface region. For example, in the problem of the magnetization at the surface of a ferromagnet, if at the surface layer the magnetization differs from the bulk by an amount $\Delta\mu_s$, the penetration of the disturbance at a distance z from the surface is given by[19–21]

$$\Delta\mu(z)=\Delta\mu_s \exp(-z/\xi) , \tag{83}$$

where ξ is a magnetic coherence length, and both $\Delta\mu_s$ and ξ are temperature dependent. Equations (31) and (82) can be immediately applied to this system, with ξ replacing λ. Indeed, polarized neutron reflectometry has been shown to be a sensitive probe to determine the temperature dependence of the magnetization at the surface of ferromagnets.[19]

ACKNOWLEDGMENTS

We would like to thank W. L. Clinton, R. A. Ferrell, C. J. Lobb, C. F. Majkrzak, and S. K. Satija for helpful conversations. The research at Maryland was supported by the NSF, Grant No. DMR 89-21878. We would also like to thank G. Ljungdahl for a critical reading of the manuscript, and in particular for his assistance with the calculation of the thick-film case.

[1] G. P. Felcher, R. T. Kampwirth, K. E. Gray, and Roberto Felici, Phys. Rev. Lett. **52**, 1539 (1984).
[2] G. P. Felcher, Roberto Felici, R. T. Kampwirth, and K. E. Gray, J. Appl. Phys. **57**, 3789 (1985).
[3] R. Felici, J. Penfold, R. C. Ward, E. Olsi, and C. Matacotta, Nature (London) **329**, 523 (1987).
[4] A. Mansour, R. O. Hilleke, G. P. Felcher, R. B. Laibowitz, P. Chaudhari, and S. S. P. Parkin, Physica B **156 & 157**, 867 (1989).
[5] K. E. Gray, G. P. Felcher, R. T. Kampwirth, and R. Hilleke, Phys. Rev. B **42**, 3971 (1990).
[6] L. P. Chernenko, D. A. Korneev, A. V. Petrenko, N. I. Balalykin, and A. V. Skripnik, in *Surface X-Ray and Neutron Scattering*, edited by H. Zabel and I. K. Robinson (Springer-Verlag, Berlin, 1992), p. 209.
[7] D. A. Korneev, L. P. Chernenko, A. V. Petrenko, N. I. Balalykin, and A. V. Skripnik, in *Neutron Optical Devices and Applications*, edited by C. F. Majkrzak and J. L. Wood (SPIE, Bellingham, WA, 1992), p. 254.
[8] Huai Zhang and J. W. Lynn, Phys. Rev. Lett. **70**, 77 (1993).
[9] G. E. Bacon, *Neutron Diffraction*, 3rd ed. (Oxford University Press, Oxford, 1975), pp. 155 and 521.
[10] F. London and H. London, Proc. R. Soc., London Ser. A **149**, 71 (1935); F. London and H. London, Physica **2**, 341 (1935).

[11]M. Tinkham, *Introduction to Superconductivity* (McGraw-Hill, New York, 1975).
[12]C. F. Majkrzak, Physica B **173**, 75 (1991).
[13]R. Golub, D. Richardson, and S. K. Lamoreaux, *Ultracold Neutrons* (Hilger, Bristol, 1991).
[14]A. Erdelyi, *Higher Transcendental Functions* (McGraw-Hill, New York, 1953), Chap. 4.
[15]F. A. Jenkins and H. E. White, *Fundamentals of Optics* (McGraw-Hill, New York, 1950), p. 254.
[16]L. D. Landau and E. M. Lifshitz, *Quantum Mechanics, Nonrelativistic Theory* (Pergamon, London, 1958), Chap. 3.
[17]G. Ljungdahl (private communication).
[18]For a review of other exact solutions related to reflection measurements, see, for example, J. Lekner, *Theory of Reflection of Electromagnetic and Particle Waves* (Nijhoff, Dordrecht, 1987), Chap. 2. For other exact solutions with potentials composed of exponential functions, see Ref. 16.
[19]G. P. Felcher, Phys. Rev. B **24**, 1595 (1981).
[20]T. Wolfram and R. E. De Wames, *Progress in Surface Science* (Pergamon, Oxford, 1975), Vol. 2, p. 233.
[21]S. F. Alvarado, Z. Phys. B **33**, 51 (1979).

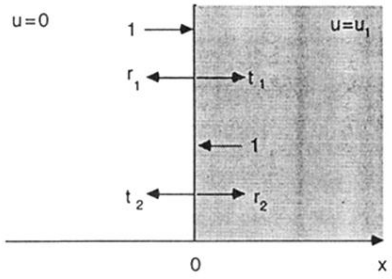

(a)

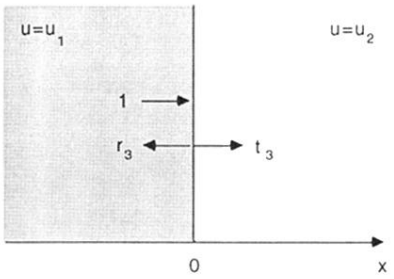

(b)

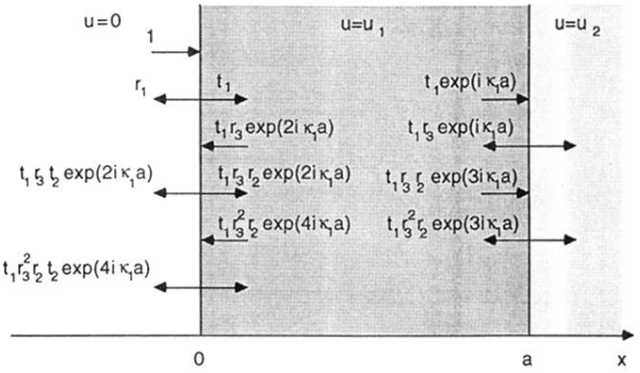

FIG. 7. Reflection and transmission of a plane wave at the first (a) and second (b) boundary, and the schematic diagram of multiple reflections (c). (r_1,t_1), (r_2,t_2), and (r_3,t_3) are the reflection and transmission amplitudes obtained with respect to the x-axis origin chosen as in (a) and (b). In (c) the reflection amplitues on the $x<0$ side compose a geometric series and the sum of the series is identical to the exact solution. The attenuation factor of the series is $r_2r_3\exp(2i\kappa_1 a)$ due to "bouncing" once from each boundary and traveling a distance $2a$ with a wave vector κ_1.

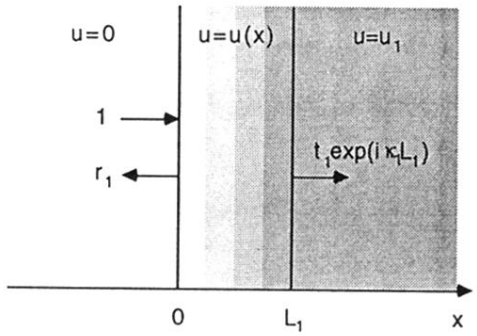

(a)

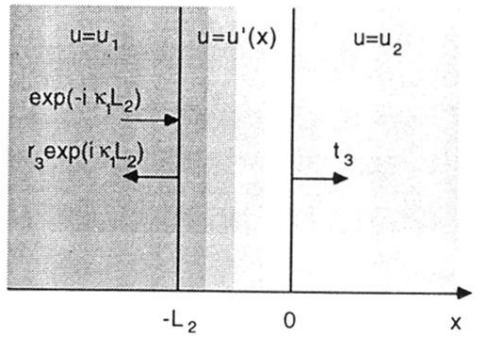

(b)

FIG. 8. Reflection and transmisson of a plane wave at the first (a) and the second (b) boundary blocks, rather than boundary planes. (r_1,t_1) and (r_3,t_3) are the reflection and transmission amplitudes obtained with respect to the x-axis origin chosen as in (a) and (b). Constant potentials and plane wave solutions are assumed outside the blocks.

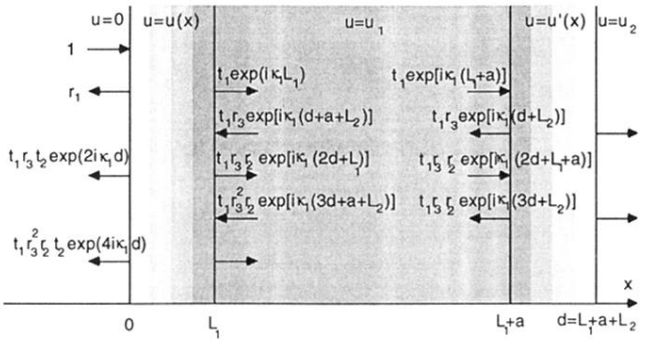

FIG. 9. Schematic diagram of multiple reflections from two boundary blocks. The attenuation factor for the multiple reflections on the $x<0$ side is $r_1 r_3 \exp(2i\kappa_1 d)$, where $d=L_1+a+L_2$ is the thickness of the film.